Cardiovascular Diabetology

RESEARCH

Open Access

Bone marrow mesenchymal stem cell-derived extracellular vesicles alleviate diabetes-exacerbated atherosclerosis via AMPK/mTOR pathway-mediated autophagy-related macrophage polarization

Libo Liu[1,2†], Ziyu An[1†], Huan Zhang[1], Xueqi Wan[1], Xin Zhao[1], Xueyao Yang[1], Jinfan Tian[1*] and Xiantao Song[1*]

Abstract

Introduction Bone marrow-derived mesenchymal stem cell-derived extracellular vesicles (BMSC-EVs) are widely used for therapeutic purposes in preclinical studies. However, their utility in treating diabetes-associated atherosclerosis remains largely unexplored. Here, we aimed to characterize BMSC-EV-mediated regulation of autophagy and macrophage polarization.

Methods EVs were isolated from the supernatant of cultured BMSCs and characterized with transmission electron microscopy (TEM), nanoparticle tracking analysis (NTA), and western blotting. A diabetes-related atherosclerotic ApoE$^{-/-}$ mouse model was established through feeding with a high-fat diet (HFD) and streptozotocin (STZ). Histopathological analyses were carried out using Oil Red O, H&E, and Masson staining of the aorta. TEM and immunohistochemistry (IHC) were applied to evaluate autophagy, and immunofluorescence (IF) was used to identify macrophage polarization. RAW264.7 macrophages were induced with oxidized low-density lipoprotein (ox-LDL) and high glucose (HG), co-cultured with BMSC-EVs, and analyzed for macrophage proliferation, migration, and foam cell formation. RAW264.7 cells were transduced with autophagy marker mRFP-GFP-LC3 lentivirus and analyzed with IF and western blotting.

Results Diabetic mice (DA group) had larger aortic plaque areas and lower collagen content than the HFD mice. BMSC-EV treatment significantly reduced blood glucose, LDL levels, and aortic plaque areas while increasing collagen content. BMSC-EV-treated aortas contained a higher number of autophagosomes/autolysosomes, with increased expression of LC3BII correlating with decreased P62 levels and a lower proportion of M1 macrophages. In vitro, BMSC-

†Libo Liu and Ziyu An contributed equally to this work and are sharing first authorship.

*Correspondence:
Jinfan Tian
tjfbama@mail.ccmu.edu.cn
Xiantao Song
song0929@mail.ccmu.edu.cn

Full list of author information is available at the end of the article

EVs inhibited proliferation, migration, and foam cell formation in ox-LDL and HG-induced activated RAW264.7 cells. These effects were reversed by the autophagy blocker bafilomycin A1. Consistent with the in vivo findings, BMSC-EVs elevated levels of the autophagy-related protein LC3BII/I and decreased P62 in ox-LDL and HG-induced RAW264.7 cells. These cells also expressed the M1 macrophage markers CD86 and iNOS, but showed reduced expression of the M2 marker Arg-1. Further, BMSC-EVs decreased AMPKα and mTOR phosphorylation levels, which were blocked by the AMPK inhibitor compound C.

Conclusions BMSC-EVs attenuate diabetes-exacerbated atherosclerosis by inhibiting vascular macrophage proliferation, migration, and foam cell formation via AMPK/mTOR signaling-regulated autophagy and macrophage polarization. BMSC-EVs thus hold promise as therapeutic agents for atherosclerosis.

Keywords Diabetes, Atherosclerosis, Bone marrow mesenchymal stem cell-derived extracellular vesicles, Autophagy, Macrophage polarization, AMPK/mTOR pathway

Graphical Abstract

Extracellular vesicles derived from bone marrow mesenchymal stem cells may mitigate diabetes-aggravated atherosclerosis by regulating AMPK/mTOR-mediated autophagy-related macrophage polarization and inhibiting macrophage proliferation, migration, foam cell formation, and cholesterol transport.

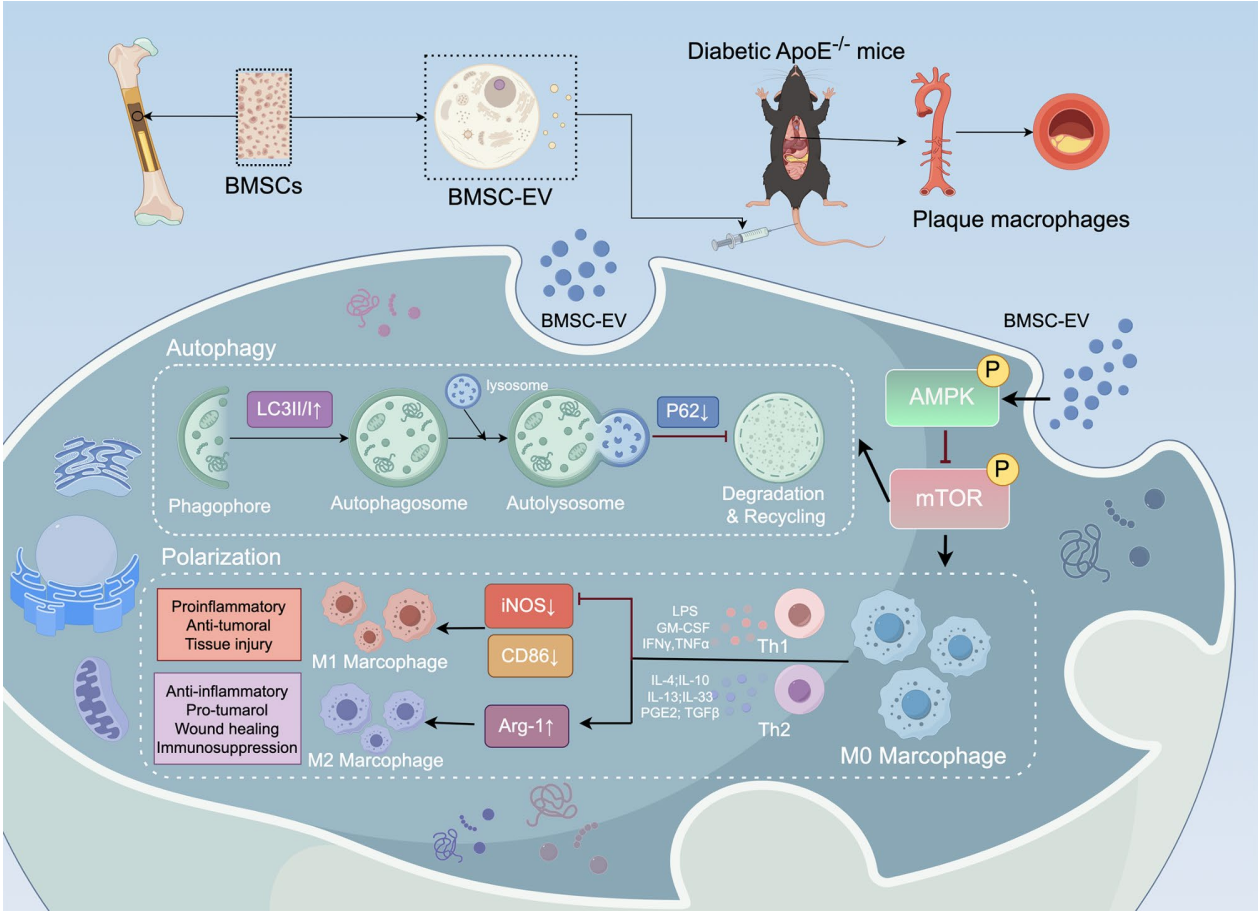

Introduction

Atherosclerotic cardiovascular disease (ASCVD) is the leading cause of global mortality, accounting for approximately one-third of all deaths worldwide (https://www.who.int/news-room/fact-sheets/detail/cardiovascular-diseases-(cvds)). Diabetes significantly exacerbates ASCVD morbidity and mortality. The recent CAPTURE study showed that nearly one-third of patients with type 2 diabetes (T2DM) have cardiovascular disease, and that approximately 90% of these cases are atherosclerotic cardiovascular diseases [1]. Although several new anti-atherosclerotic drugs have been incorporated into clinical practice, therapeutic strategies that primarily target LDL reduction still present a residual risk of cardiovascular

disease [2]. Drugs targeting alternative anti-atherosclerotic pathways are urgently needed, particularly for patients with comorbid T2DM and ASCVD.

Macrophages are hyperactive in atherosclerotic lesions, and macrophage-derived foam cells form the core of atherosclerotic plaques. Foam cell formation and progression are closely linked to autophagy [3]. Autophagy, a lysosome-mediated cellular degradation pathway, is critical to the maintenance of cellular nutrient balance and organelle functioning. In the early stages of atherosclerosis, macrophage autophagy inhibits foam cell formation and mitigates atherosclerotic progression. However, as atherosclerosis advances, macrophage autophagy becomes impaired, leading to increased foam cell formation and accelerated disease progression [4]. Thus, promoting macrophage autophagy in the early stages of atherosclerosis may protect against further disease development [5].

Atherosclerotic lesions begin with the accumulation of pro-inflammatory M1 macrophages in the arterial intima. These macrophages have inefficient lipid metabolism and are thus the primary source of foam cells. Cholesterol, advanced glycation end-products (AGEs) from hyperglycemia, and oxidized low density lipoproteins (xo-LDL) can all stimulate M1 macrophages to secrete pro-inflammatory cytokines (e.g., TNF-α, IL-1β, IL-6, IL-12, and IL-23), further exacerbating atherosclerosis. Conversely, M2 macrophages produce anti-inflammatory cytokines (e.g., IL-10 and TGF-β) and have anti-atherogenic effects. Emerging evidence suggests that autophagy regulates macrophage polarization, in part via suppression of M1 pro-inflammatory macrophages, which reduces inflammation [6, 7]. However, the precise molecular mechanisms by which autophagy influences macrophage polarization remain unclear.

The mechanistic target of rapamycin (mTOR) is a key regulator of autophagy and macrophage polarization, suggesting it may play a critical role in autophagy-mediated regulation of macrophage polarization [8–10]. AMP-activated protein kinase (AMPK), an upstream signaling molecule for mTOR, has been found to play a significant role in T2DM and other metabolism-related diseases. Recent research suggests that AMPK-mediated regulation of mTOR signaling confers cytoprotective effects by inducing macrophage autophagy and promoting M2 macrophage polarization [11, 12].

Extracellular vesicles (EVs) are produced by mammalian cells and have significant potential as therapeutic agents, particularly in stem cell therapy. Compared to their parental cells, EVs are safer and easier to produce, store, transport, and administer [13]. Previous work has shown that mesenchymal stem cells (MSC-EVs) can alleviate T1DM via upregulation of β-cell autophagy [14]. MSC-EVs and their associated microRNAs can modulate macrophage polarization and reduce atherosclerotic progression [15, 16]. Despite these promising findings, however, the mechanisms underlying MSC-EVs' protective effects remain poorly understood.

In this study, we investigated the effects of BMSC-EVs on atherosclerosis in diabetic $ApoE^{-/-}$ mice, as well as their impact on RAW264.7 cells and signaling pathways. We found that BMSC-EVs alleviated diabetes-accelerated atherosclerosis by modulating autophagy-mediated macrophage polarization. BMSC-EVs may offer a novel strategy for MSC-based treatment of diabetes-associated atherosclerosis.

Materials and methods

Cells

Primary BMSCs were isolated from C57BL/6J mice. Mice, all male and aged 3–4 weeks, were obtained from Beijing HFK Bio-technology Co., Ltd. (Beijing, China) (Permission No. SCXK(Jing) 2019-0008). Mice were sacrificed by cervical dislocation and were then immersed in 75% ethanol for 5 min for disinfection. Femurs and tibias were aseptically isolated and placed in pre-cooled phosphate-buffered saline (PBS; Cytiva, SH30256) containing 1% penicillin–streptomycin (P–S) suspension (Gibco, 15140122). Both ends of the femurs and tibias were excised to explore the medullary cavities. Cavities were flushed with Dulbecco's Modified Eagle Medium/Nutrient Mixture F-12 (DMEM/F-12; Gibco, 11320033) supplemented with 20% fetal bovine serum (FBS) (Hyclone, SH30406.05) and 1% P/S using a 1 mL, 25G syringe. Flushed bone marrow was collected, homogenized with pipettes, and filtered through a 75-μm cell strainer to obtain single-cell suspensions. Cellular suspensions were carefully layered onto Ficoll-Paque PREMIUM (Cytiva, 17544602) at a ratio of 1:3 and centrifuged at 400 g for 5 min at 4 °C. The middle layer was then aspirated, and 5 mL of the above complete culture medium was added to the suspension. This mixture was centrifuged again at 400 g for 5 min at 4 °C. The resulting cell pellet was resuspended and inoculated into a T25 cell culture flask and then incubated at 37 °C with 5% CO_2. After 24 h, supernatant containing non-adherent cells was aspirated and discarded. A fresh complete medium was then added, and the culture was continued. The medium was changed first after 72 h, and subsequently every 48 h. When the cells reached approximately 80% confluency, they were digested with 0.25% Trypsin–EDTA (Gibco, 25200056) and passaged. Cells from the third passage were used for further experiments. For detailed BMSC isolation and culture procedures, please refer to Supplementary Fig. 1A.

RAW264.7 mouse macrophages were purchased from Procell Life Science & Technology Co., Ltd. (CL-0190, Wuhan, China). They were cultured in high-glucose Dulbecco's Modified Eagle Media (DMEM; Gibco, 11965092) containing 10% FBS and 1% P–S. To prepare for induction

of RAW264.7 cells, D-(+)-glucose (Sigma, 50-99-7) was added to glucose-free DMEM media (Gibco, 11966025) to achieve a final glucose concentration of 33.3 mmol/L. Ox-LDL was then added to the high-glucose media to adjust the final concentration to 75 μg/mL.

Animals and groups

All experimental procedures involving animals were conducted in strict accordance with the National Institutes of Health Guidelines for the Use of Laboratory Animals and were approved by the Animal Experiment Center of the Beijing Anzhen Hospital Ethics Committee, which is affiliated with Capital Medical University (Approval Number: 2022152X). Eight-week-old male wildtype C57BL/6J mice and ApoE$^{-/-}$ mice with C57BL/6J backgrounds were procured from Beijing Vital River Company (Permission No. SCXC(Jing) 2021-0006). A Western diet was obtained from Beijing HFK Biotechnology Co., Ltd. (HFK, H10141). Mice were housed in the specific pathogen-free (SPF) animal facility at Beijing Anzhen Hospital. The mice were kept under 12-h light/dark cycles at a consistent temperature and humidity. To establish a mouse model of comorbid diabetes mellitus and atherosclerosis, ApoE$^{-/-}$ mice were initially fed a standard diet for two weeks, followed by a four-week high-fat diet (HFD) to induce insulin resistance. Hyperglycemia was induced via intraperitoneal (i.p.) injections of streptozotocin (STZ) (Aladdin, S110910) at a dose of 50 mg/kg/day for three consecutive days.

ApoE$^{-/-}$ mice with fasting blood glucose levels ≥ 8.6 mmol/L (determined with rapid blood glucose test strips (Roche, CN-RET-824) [17], were deemed to have successfully developed diabetes and were included in subsequent experiments.

The selected mice were split into eight groups: a wild type (WT) group (C57BL/6J, n = 10), an ordinary diet (OD) group (ApoE$^{-/-}$, n = 10), a HFD group (ApoE$^{-/-}$, n = 10), a diabetic (DA) group (STZ induced ApoE$^{-/-}$, n = 10), a Rapamycin (RAPA) group (STZ induced ApoE$^{-/-}$, n = 10), a PCSK9i group (STZ induced ApoE$^{-/-}$, n = 10), a BMSC group (STZ induced ApoE$^{-/-}$, n = 10), and a BMSC-EV group (STZ induced ApoE$^{-/-}$, n = 10). After the successful model establishment, six surviving mice were selected from each group for final experiments.

Subsequent interventions were conducted as follows: The RAPA group received i.p. doses of rapamycin (MCE, HY10291) at a dose of 1 mg/kg/day. The PCSK9i group received subcutaneous (s.c.) injections with SBC-115076 (MCE, HY12402) at a dose of 4 mg/kg/day. The BMSC group received transcaudal intravenous (i.v.) injections of 2×10^6 cells twice a week, and the BMSC-EV group received tail vein injections with 200 μL (100 μg) of BMSC-EVs twice a week. The WT group and OD group continued to receive ordinary diets. The remaining groups were also administered an equivalent i.p. volume of physiological saline as a control. A schematic

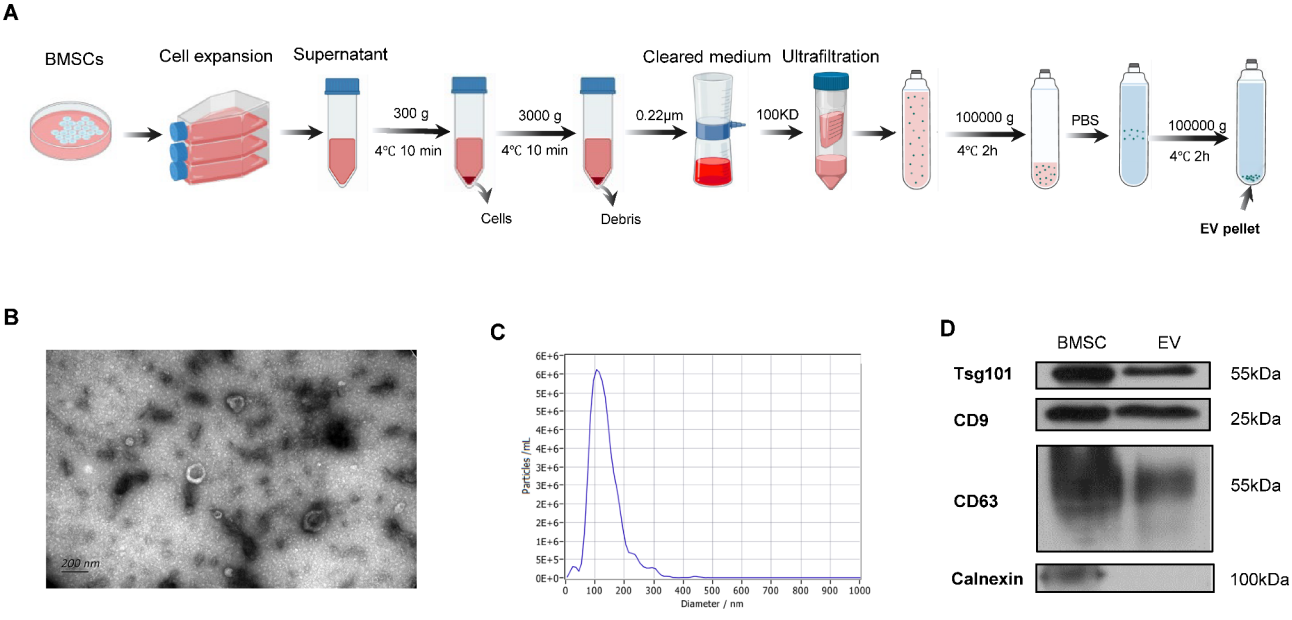

Fig. 1 Isolation and Characterization of BMSC-EV. **A** Schematic representation of BMSC-EV isolation from cellular supernatants using a combination of ultrafiltration and ultracentrifugation techniques. **B** TEM image showing the distinctive cup-shaped morphology of the isolated BMSC-EV. **C** NTA depicting the size distribution profile of the BMSC-EV population. **D** Western blots showing the presence of surface protein markers specific to BMSC-EV. Abbreviations: BMSC-EV, extracellular vesicles derived from bone marrow mesenchymal stem cells; TEM, transmission electron microscope; NTA, nanoparticle tracking analysis

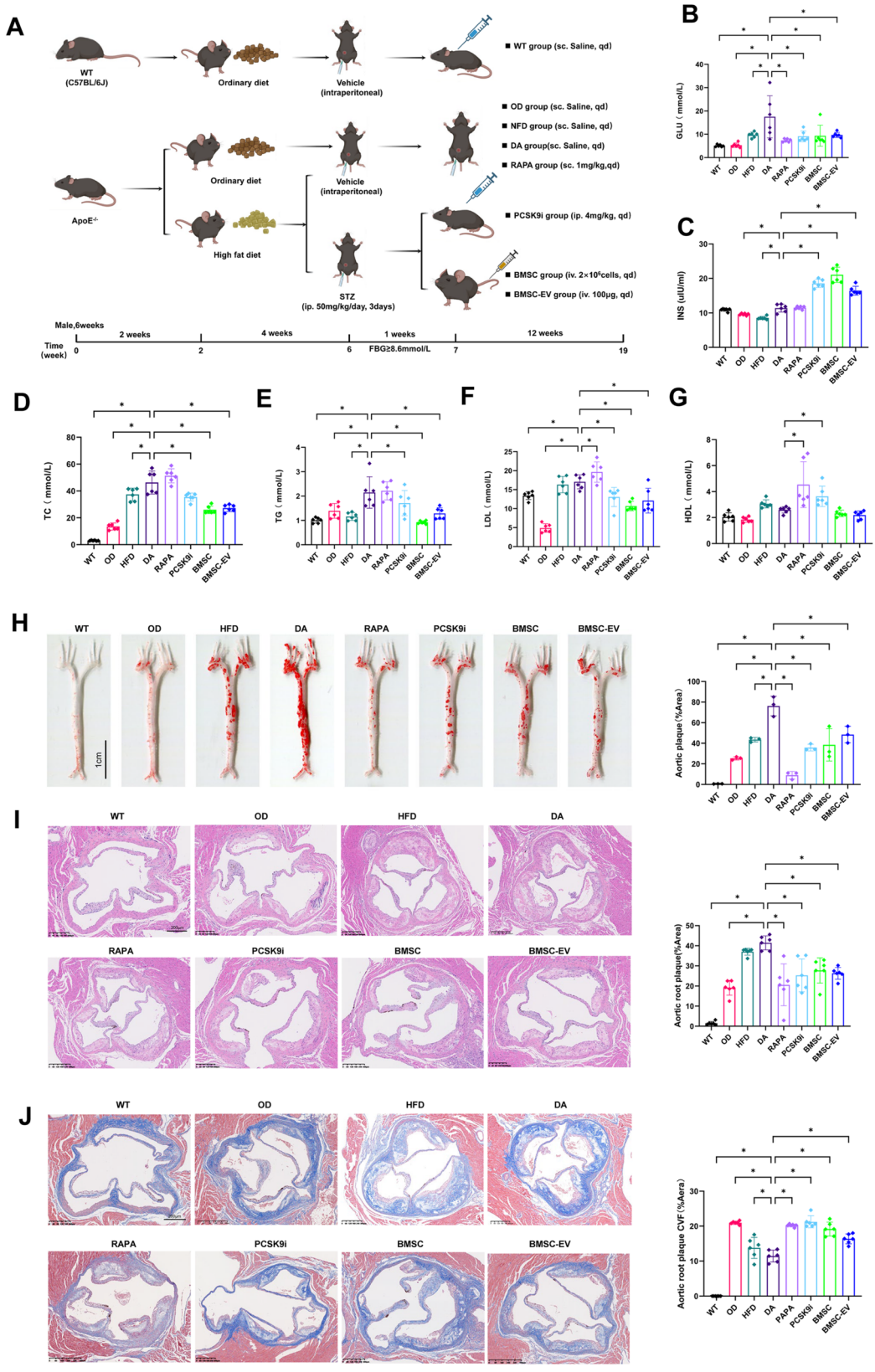

Fig. 2 (See legend on next page.)

(See figure on previous page.)

Fig. 2 Effects of Different Interventions on Blood Lipid Profiles and Aortic Atherosclerosis in Diabetic ApoE$^{-/-}$ Mice. **A** Flowchart depicting the establishment of animal models and group dosing. **B–G** After 19 weeks of intervention, blood glucose levels were assessed with a rapid blood glucose meter, and serum insulin and blood lipid profiles were determined via biochemical methods (n = 6). **H** Oil Red O staining illustrates the distribution of atherosclerotic plaques in intact mouse aortas, along with plaque area quantification (n = 3). **I** H&E staining shows the distribution of atherosclerotic plaques in the transvalvular transverse section of the mouse aortic root, alongside quantification of plaque area. **J** Masson staining demonstrates the collagen content and ratio of collagen/plaque area in atherosclerotic plaques in the transverse axial section of the mouse aortic root (n = 6). (Pairwise comparisons between experimental groups were conducted using one-way ANOVA, * $P < 0.05$). Abbreviations: H&E staining, hematoxylin–eosin staining; WT, wild type; OD, ordinary diet; HFD, high-fat diet; DA, diabetes-accelerated atherosclerosis; RAPA, rapamycin; PCSK9i, proprotein convertase subtilisin/kexin type 9 inhibitor; BMSC, bone marrow mesenchymal stem cells; BMSC-EV, extracellular vesicles derived from bone marrow mesenchymal stem cells

representation of the mouse models and group interventions is depicted in Fig. 2A.

Statistical analysis

Statistical analyses were conducted using GraphPad Prism 10.0 (GraphPad, La Jolla, CA, USA). All data were collected from at least three independent experiments and are presented as means ± standard deviations (SDs). Between-group differences were analyzed using a one-way analysis of variance (ANOVA), followed by LSD-t post hoc analysis. A *P*-value of less than 0.05 was considered statistically significant.

A comprehensive list of experimental methods and major resources is available in the Online Supplement. The authors declare that the majority of the supporting data are included in this paper and/or its Online Data Supplement. Source data for figures, as well as additional data that are not shown, can be made available upon reasonable request to the corresponding author.

Results

Identification of mouse BMSCs and there of derived EVs

To isolate BMSC-EVs, primary mouse BMSCs were first separated using Ficoll-based density gradient centrifugation, followed by differential attachment methods (Supplementary Fig. 1A). Cells were then examined under a light microscope. On the second culture day, smaller colonies with uneven morphology began to form (Supplementary Fig. 1B, P0-2 day). By the fifth day, the colonies had expanded, merged, and showed central cell stacking (Supplementary Fig. 1B, P0-5 day). After passage, the cells displayed typical polygonal fibroblast-like morphology, including more uniform appearances (Supplementary Fig. 1B, P1-7-day).

To assess the cells multi-lineage differentiation potentials, adipogenic, osteogenic, and chondrogenic differentiation was induced. Oil Red O staining demonstrated the formation of lipid droplets after two weeks of adipogenic induction (Supplementary Fig. 1C, Adipogenic). Alizarin Red staining showed significant ossification nodules after two weeks of osteogenic induction (Supplementary Fig. 1C, Osteogenic). Alicin Blue staining, performed after three weeks of chondrogenic induction, revealed blue-stained cytoplasm components within the formed cell clumps, indicating chondrogenic differentiation (Supplementary Fig. 1C, Chondrogenic).

Flow cytometry analysis was also conducted to detect the expression of specific BMSC cell surface markers. The results showed that the cellular population was positive for several mesenchymal stem cell markers, including CD44 (99.7%), CD29 (98.8%), and Sca-1 (98.8%), but was negative for CD31 (0.3%), CD117 (0.5%), and CD34 (27.3%) (Supplementary Fig. 1D).

After BMSCs were passaged and expanded, cell culture supernatants were collected. EVs were isolated using ultrafiltration and low-temperature ultracentrifugation (Fig. 1A). EVs were identified based on their morphologies, particle size distribution, and surface molecule expression using transmission electron microscopy (TEM), nanoparticle tracking analysis (NTA), and western blots.

TEM images revealed scattered "saucer-like" structures with convex peripheries and concave centers, all of which are typical EV characteristics (Fig. 1B). NTA results indicated that the vesicles had an average particle size of 134.4 ± 75.1 nm, with the main peak (at 114.2 nm) accounting for 99.3% of the particles and a concentration of 5.8×10^{10} particles/mL (Fig. 1C). Western blots showed that EVs expressed TSG101, CD9, and CD63, but not calnexin. In contrast, calnexin was detected in BMSC lysates (Fig. 1D).

High glucose states exacerbate atherosclerosis in vivo and foam cell formation in vitro

To construct a diabetes-exacerbated atherosclerosis model, STZ was used to induce diabetes in ApoE$^{-/-}$ mice on an HFD, resulting in diabetic ApoE$^{-/-}$ mice (Fig. 2A–C). Blood lipid analysis showed that, compared to non-diabetic ApoE$^{-/-}$ mice on an HFD, the DA group had significantly increased levels of total cholesterol (TC), triglycerides (TG), and LDL ($P < 0.05$) (Fig. 2D–F).

Histological analysis of aortic atherosclerosis using Oil Red O and hematoxylin and eosin (H&E) staining showed a progressive increase in aortic plaque areas from the OD group to the HFD group, and then to the DA-aggravated atherosclerosis group (all $P < 0.05$). Additionally, Masson staining showed that collagen content, which is indicative of plaque stability, was significantly reduced in DA group

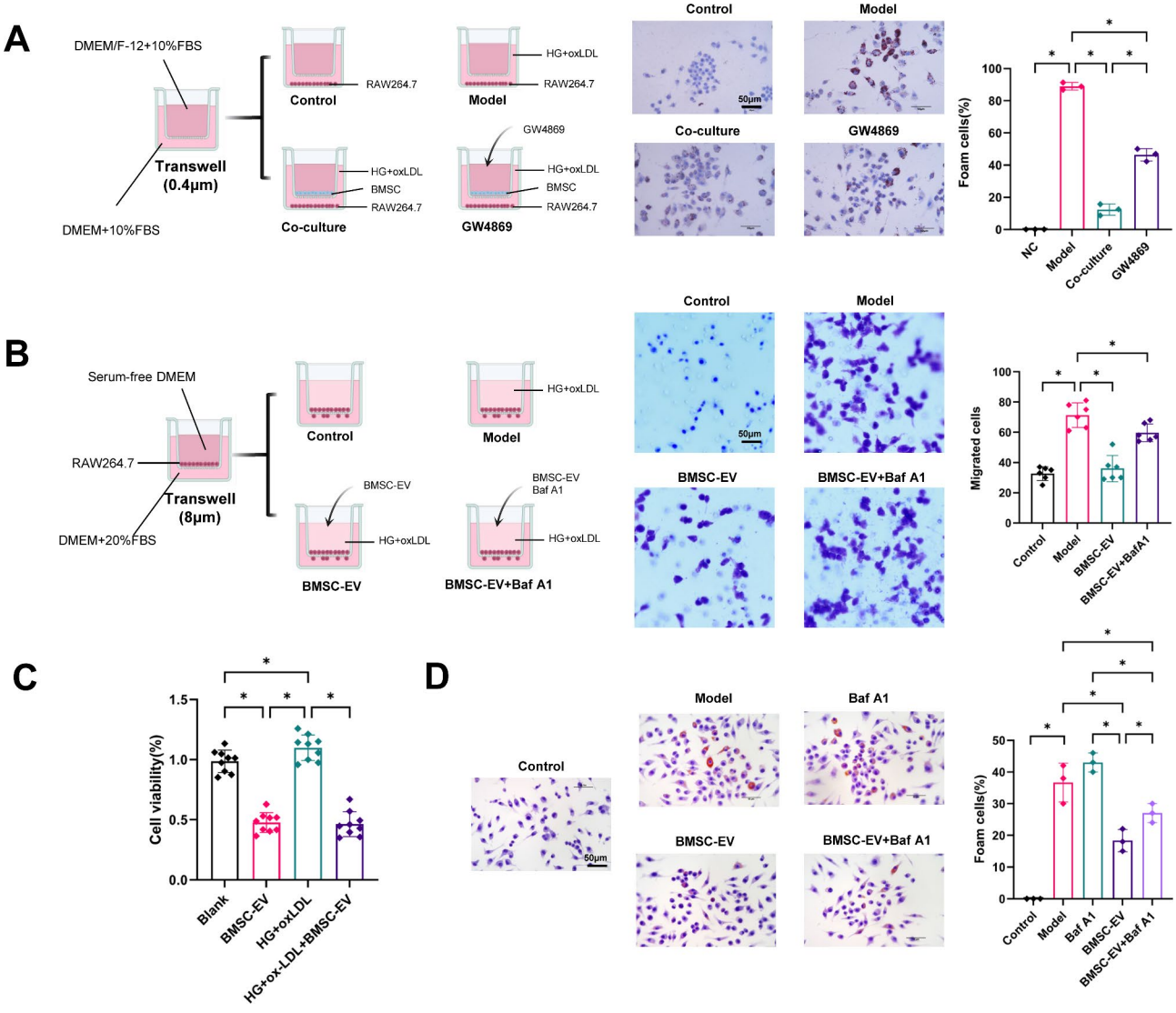

Fig. 3 Effects of BMSC-EVs on HG-ox-LDL-Induced Macrophage Proliferation, Migration, Foam Cell Formation, and Cholesterol Efflux. **A** A co-culture system of BMSC and RAW264.7 cells in Transwell chambers was constructed to evaluate the effect of BMSC-EVs on the formation of RAW264.7 foam cells using Oil Red O staining (n = 3). **B** Transwell migration assays were used to assess the effects of BMSC-EVs on RAW264.7 cell migration. **C** CCK-8 assays were used to evaluate the effects of BMSC-EVs on RAW264.7 cell proliferation (n = 9). **D** Oil Red O staining was used to evaluate the effect of BMSC-EVs on RAW264.7 foam cell formation. (Pairwise comparisons between experimental groups were performed using one-way ANOVA, * $P < 0.05$). Abbreviations: WT, wild type; OD, ordinary diet; HFD, high-fat diet; DA, diabetes-accelerated atherosclerosis; RAPA, rapamycin; PCSK9i, proprotein convertase subtilisin/kexin type 9 inhibitor; BMSC, bone marrow mesenchymal stem cells; BMSC-EV, extracellular vesicles derived from bone marrow mesenchymal stem cells; HG, high glucose; ox-LDL, oxidized low-density lipoprotein; CCK-8, Cell Counting Kit-8; BMSC, bone marrow mesenchymal stem cells; Baf A1, Bafilomycin A1

aortic plaques compared to the OD and HFD groups (all $P < 0.05$) (Fig. 2H–I).

In vitro experiments were conducted to determine the optimal concentration and exposure time for HG combined with ox-LDL in RAW264.7 cells using CCK-8 assays (Supplementary Fig. 2A-B). Oil Red O staining demonstrated that exposure to 75 μg/mL ox-LDL for 24 h induced significant foam cell formation in RAW264.7 cells. The presence of HG led to an additional increase in the foam cell proportions (Supplementary Fig. 2C).

BMSC-EVs reduce diabetes-exacerbated atherosclerosis

Serological testing revealed that the BMSC-EV group had significantly lower glucose, TC, TG, and LDL levels compared to the DA group (all $P < 0.05$). Serum insulin levels were also significantly higher in the BMSC-EV group ($P < 0.05$), but high-density lipoprotein (HDL) levels did not significantly differ between the two groups. No significant reduction in TC and TG levels was observed in the RAPA group, but the RAPA group did have higher LDL levels ($P < 0.05$). There were also no statistically

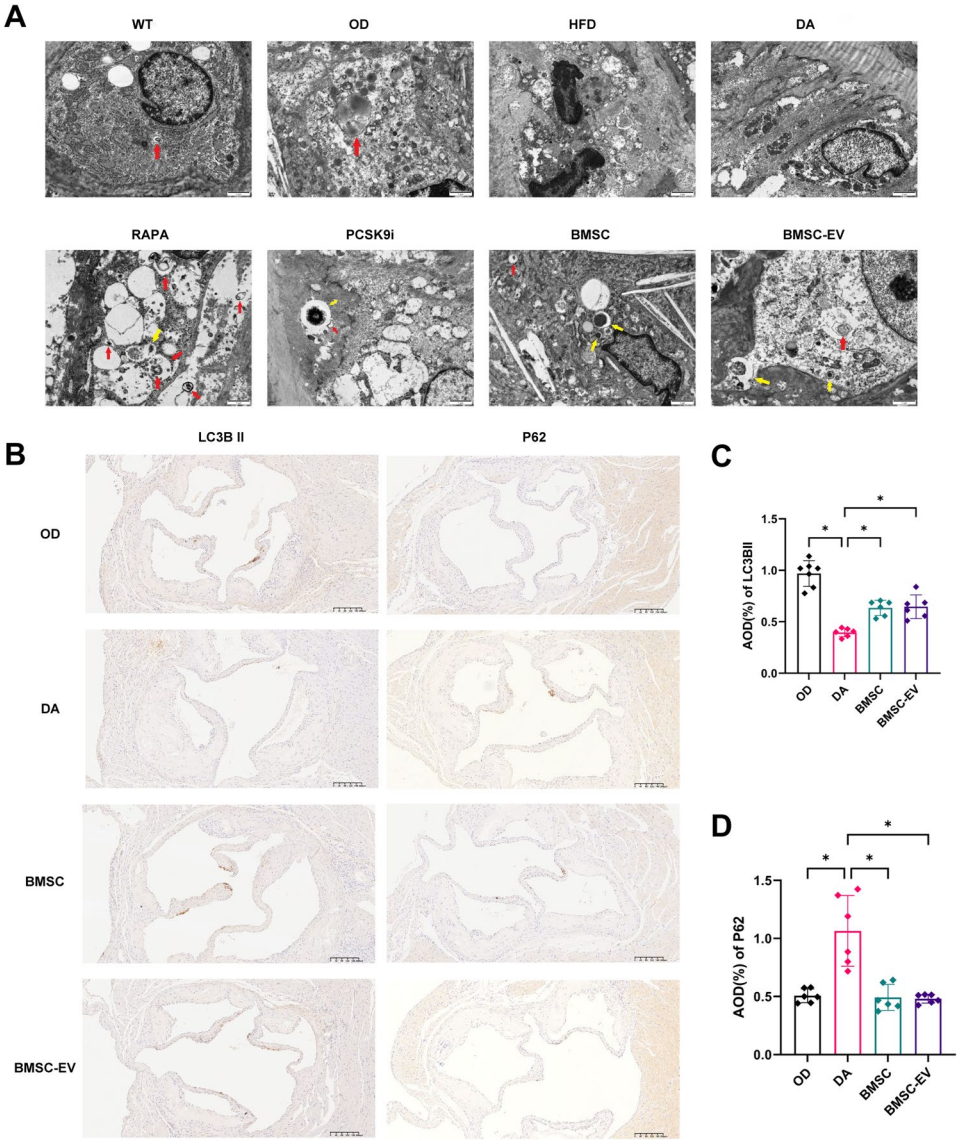

Fig. 4 BMSC-EV Regulates Autophagy In Vivo. **A** Transmission electron microscopy reveals autophagosomes (red arrows) and autolysosomes (yellow arrows) in mouse arteries, which were used to evaluate autophagy status. **B–D** Immunohistochemical staining demonstrated the effect of BMSC-EVs on the expression of autophagy-related proteins LC3BII and P62 in cells of the mouse aortic root (n = 6). (Pairwise comparisons between experimental groups were conducted using one-way ANOVA, * $P < 0.05$). Abbreviations: WT, wild type; OD, ordinary diet; HFD, high-fat diet; DA, diabetes-accelerated atherosclerosis; RAPA, rapamycin; PCSK9i, proprotein convertase subtilisin/kexin type 9 inhibitor; BMSC, bone marrow mesenchymal stem cells; BMSC-EV, extracellular vesicles derived from bone marrow mesenchymal stem cells; P62, prostacyclin; LC3B, microtubule-associated protein. AOD, Average Optical Density

significant differences in TC, TG, or LDL levels between the PCSK9i and BMSC-EV groups ($P > 0.05$) (Fig. 2A–G).

To determine the effects of BMSC-EVs on diabetes-exacerbated atherosclerosis, we administered BMSC-EVs to diabetic ApoE$^{-/-}$ mice and evaluated their arteries using Oil Red O staining of the aorta, as well as H&E and Masson staining of the aortic roots. We found a significant reduction in aortic plaque area and a notable increase in plaque collagen content in the BMSC-EV group compared to the DA group (all $P < 0.05$) (Fig. 2H–J).

Taken together, these findings suggest that BMSC-EVs can effectively reduce the severity of atherosclerosis and enhance plaque stability in diabetic conditions.

BMSC-EVs inhibit RAW264.7 cellular migration, proliferation, and foam cell formation

To understand the cellular mechanisms underlying BMSC-EVs' alleviation of diabetes-accelerated atherosclerosis, we first established a co-culture system of BMSCs and RAW264.7 cells. Oil Red O staining revealed

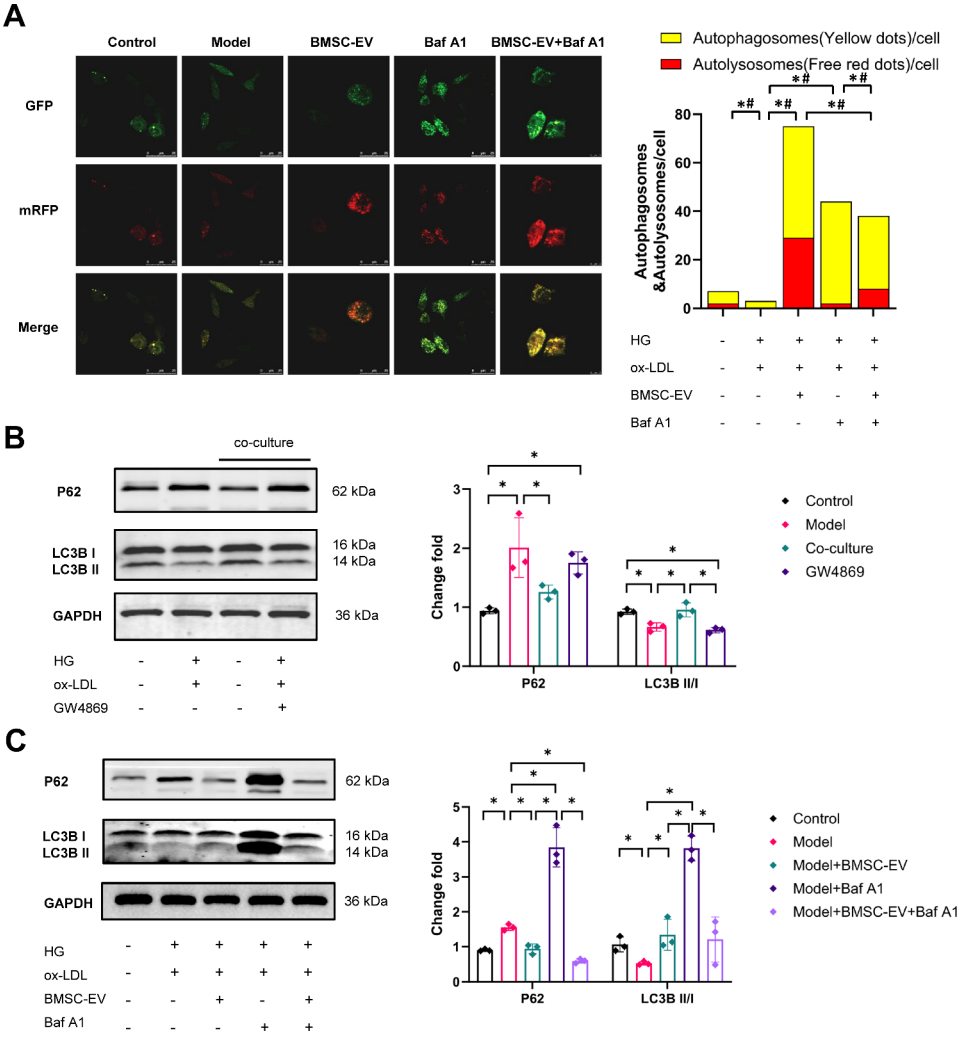

Fig. 5 BMSC-EV Regulates Autophagy In Vitro. **A** After transfection of mRFP-GFP-LC3 autophagy double-labeled lentivirus into RAW264.7 cells, laser confocal microscopy was used to assess the effect of BMSC-EV on autophagy flow. (Red dots, autolysosomes; Yellow dots, autophagosomes; *Statistical difference between the sum of red points and yellow points. # Statistical difference in the proportion of red points to the total number of points.) **B** Using a Transwell-based co-culture system of BMSC and RAW264.7 cells, Western blots were used to evaluate the effect of BMSC on macrophage autophagy (n = 3). **C** Western blots showed the effect of BMSC-EV on macrophage autophagy (n = 3). (Pairwise comparisons between experimental groups were conducted using one-way ANOVA, * $P < 0.05$, # $P < 0.05$). Abbreviations: BMSC-EV, extracellular vesicles derived from bone marrow mesenchymal stem cells; HG, high glucose; ox-LDL, oxidized low-density lipoprotein; Baf A1, Bafilomycin A1; P62, prostacyclin; LC3B, microtubule-associated protein

a significant reduction in the proportion of macrophages forming foam cells in the co-culture group compared to the model group ($P < 0.05$) (Fig. 3A). The proportion of foam cells significantly increased when cells were treated with the EV secretion inhibitor GW4869 ($P < 0.05$) (Fig. 3A).

We next used Transwell chambers, CCK-8 assays, and Oil Red O staining to assess the effects of BMSC-EVs on macrophage migration, proliferation, and foam cell formation. Results indicated that macrophage migration, proliferation activity, and foam cell formation were all significantly elevated in the model group compared to the control group (all $P < 0.05$). However, these parameters were significantly reduced in the BMSC-EVs treatment group compared to the model group ($P < 0.05$) (Fig. 3B, C). Notably, reductions in foam cell formation were reversed following the administration of the autophagy blocker bafilomycin A1 (Baf A1) in the respective groups ($P < 0.05$) (Fig. 3D).

BMSC-EV regulates macrophage autophagy

To further explore BMSC-EVs' effects on autophagy, we used TEM to evaluate autophagosomes and autophagolysosomes in mouse aortas. Autophagosomes and autophagolysosomes were seen in the visual fields in the DA, OD, RAPA, PCSK9i, BMSC, and BMSC-EV groups. Typical autophagosomes and autophagolysosomes were rarely observed in the HFD and DA groups,

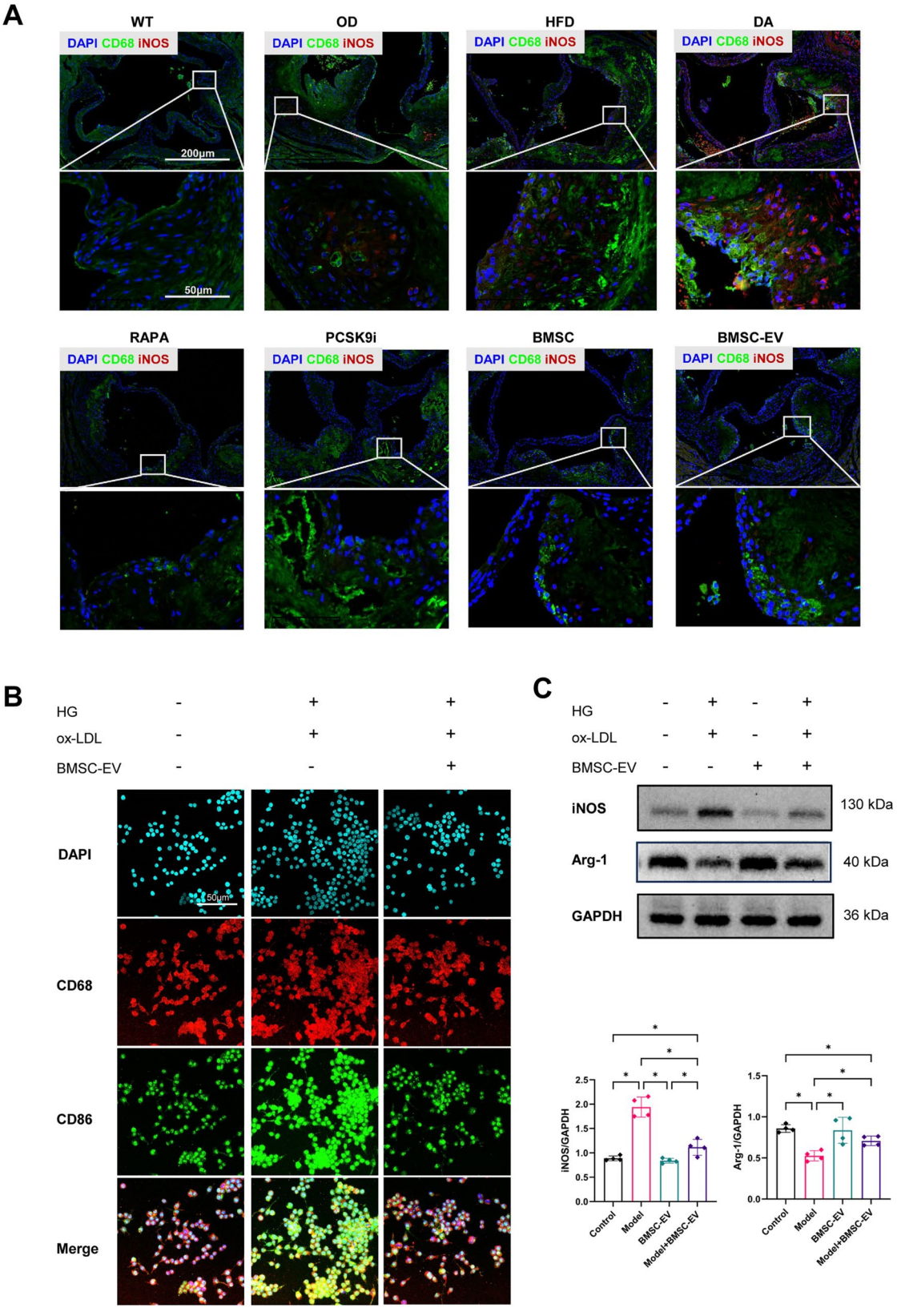

Fig. 6 (See legend on next page.)

(See figure on previous page.)

Fig. 6 BMSC-EV Modulates Macrophage Polarization Phenotype In Vivo and In Vitro. **A** Immunofluorescence (IF) co-staining illustrates M1 macrophages (CD68 & iNOS positive) within atherosclerotic plaques in the transvalvular section of the mouse aortic root. (Blue, DAPI; Green, CD68; Red, iNOS). **B** IF shows the effects of BMSC-EV on M1 polarization of RAW264.7 macrophages induced by HG combined with ox-LDL. Green fluorescence intensity indicates the expression level of the M1 polarization marker molecule CD86. **C** Western blots showing the effects of BMSC-EV on the relative expression of the M1-type polarization marker molecule iNOS and M2-type polarization marker molecule Arg-1 in RAW264.7 macrophages induced by HG combined with ox-LDL (n = 3). (Pairwise comparisons between experimental groups were conducted using one-way ANOVA, *$P < 0.05$). Abbreviations: DAPI, 4,6-diamidino-2-phenylindole; iNOS, inducible nitric oxide synthase; WT, wild type; OD, ordinary diet; HFD, high-fat diet; DA, diabetes-accelerated atherosclerosis; RAPA, Rapamycin; PCSK9i, Proprotein Convertase Subtilisin/Kexin Type 9 inhibitor; BMSC, bone marrow mesenchymal stem cells; BMSC-EV, extracellular vesicles derived from bone marrow mesenchymal stem cells; Arg-1, Arginase-1; IF, Immunofluorescence

suggesting inhibited autophagy. In the RAPA group, in contrast, multiple autophagosomes (Fig. 4A, red arrow) and autophagolysosomes (Fig. 4A, yellow arrow) were evident, indicating active autophagy. We also performed immunohistochemical (IHC) staining to assess the expression of autophagy-related proteins LC3B and P62 in mouse aortic root tissue. Compared with the OD group, the DA model group showed a significant increase in P62 expression and a decrease in LC3B II expression ($P < 0.05$). The BMSC and BMSC-EV groups, in contrast, showed reduced P62 but increased LC3B II expression compared to the DA group (both $P < 0.05$). No significant difference was observed between the BMSC and BMSC-EV groups ($P > 0.05$). These findings suggest that BMSC-EV can upregulate autophagy in diabetes-related atherosclerotic tissue, exhibiting effects comparable to those of BMSC (Fig. 4B–D).

In vitro, we used the mRFP-GFP-LC3B viral reporter-based autophagy flux detection tool in RAW264.7 cells and then observed and quantified autophagosomes (red dots) and autophagolysosomes (yellow dots). There were significantly fewer autophagosomes and autophagolysosomes in the model group compared to the control group, indicating blocked autophagy flux ($P < 0.05$). In contrast, the number of autophagosomes and autophagolysosomes was significantly increased in the BMSC-EV group compared to the model group, indicating autophagy flux activation ($P < 0.05$) (Fig. 5A). In the BMSC-EV plus Baf A1 group, cells were predominantly characterized by increased proportions of yellow granular autophagosomes and decreased red autophagy lysosomes compared to the BMSC-EV group. However, the proportion of red autophagy lysosomes in the combined BMSC-EV-Baf A1 group was higher than the proportion in the Baf A1 group alone (all $P < 0.05$). This suggest that Baf A1 partially blocked BMSC-EV-induced activation of autophagy flux (Fig. 5A).

To indirectly demonstrate that BMSC-EVs are key mediators of the therapeutic effects of BMSCs, we established a transwell co-culture system of BMSCs and RAW264.7 macrophages (Fig. 3A). Compared with the control group, the model group (e.g., ox-LDL and HG-induced-RAW264.7 cells) had significantly increased expression of the autophagy-related protein P62, but significant reductions in the LC3B II/I ratio (all $P < 0.05$). In the BMSC co-culture group, P62 expression was significantly reduced, and the LC3B II/I ratio was significantly increased (all $P < 0.05$), suggesting that BMSCs upregulated autophagy processes in co-cultured RAW264.7 cells. However, after the addition of GW4869 to the BMSC culture system, there was no significant increase in autophagy in RAW264.7 cells ($P < 0.05$) (Fig. 5B).

We also directly treated RAW264.7 cells with BMSC-EVs and detected autophagy-related proteins via western blot analysis. Results indicated that, compared to the control group, P62 protein expression was significantly increased, but the LC3B II/I ratio was significantly decreased, in the model group (induced by ox-LDL and HG) (all $P < 0.05$). In the Baf A1 group, both P62 and the LC3B II/I ratio were further increased compared with the model group, indicating inhibited autophagy in the model group. However, in the BMSC-EV group, P62 protein expression was significantly decreased compared to the model group, while the LC3B II/I ratio was significantly increased (all $P < 0.05$). Administration of BMSC-EVs also reversed Baf-A1-induced increases in P62 and the LC3B II/I ratio ($P < 0.05$) (Fig. 5C).

BMSC-EVs modulate macrophage polarization phenotypes

We evaluated the proportion of M1 macrophages in atherosclerotic plaques in mouse aortic tissue using multiplex immunofluorescence (IF) staining. We found cells co-stained green (CD68-positive, macrophage marker) and red (iNOS-positive, M1 macrophage marker) in the $ApoE^{-/-}$ OD, HFD, and DA groups. The OD, HFD, and DA groups also showed an increasing trend in M1 macrophage numbers, consistent with the severity of atherosclerotic lesions. In contrast, the RAPA, PCSK9, BMSC, and BMSC-EV groups, despite showing obvious aortic root plaques, had very few iNOS-positive cells (Fig. 6A).

To further explore the impacts of BMSC-EVs on macrophage polarization phenotypes, we first performed multiple IF analyses using RAW264.7 cells. The results indicated that, compared to the control group, the fluorescence intensity of the M1 macrophage marker CD86 was significantly increased in the model group, but was decreased in the BMSC-EVs group ($P < 0.05$) (Fig. 6B). We also detected M1 polarization marker iNOS and M2 polarization marker Arg-1 expression in RAW264.7 cells using western blots. Compared to the control group, the

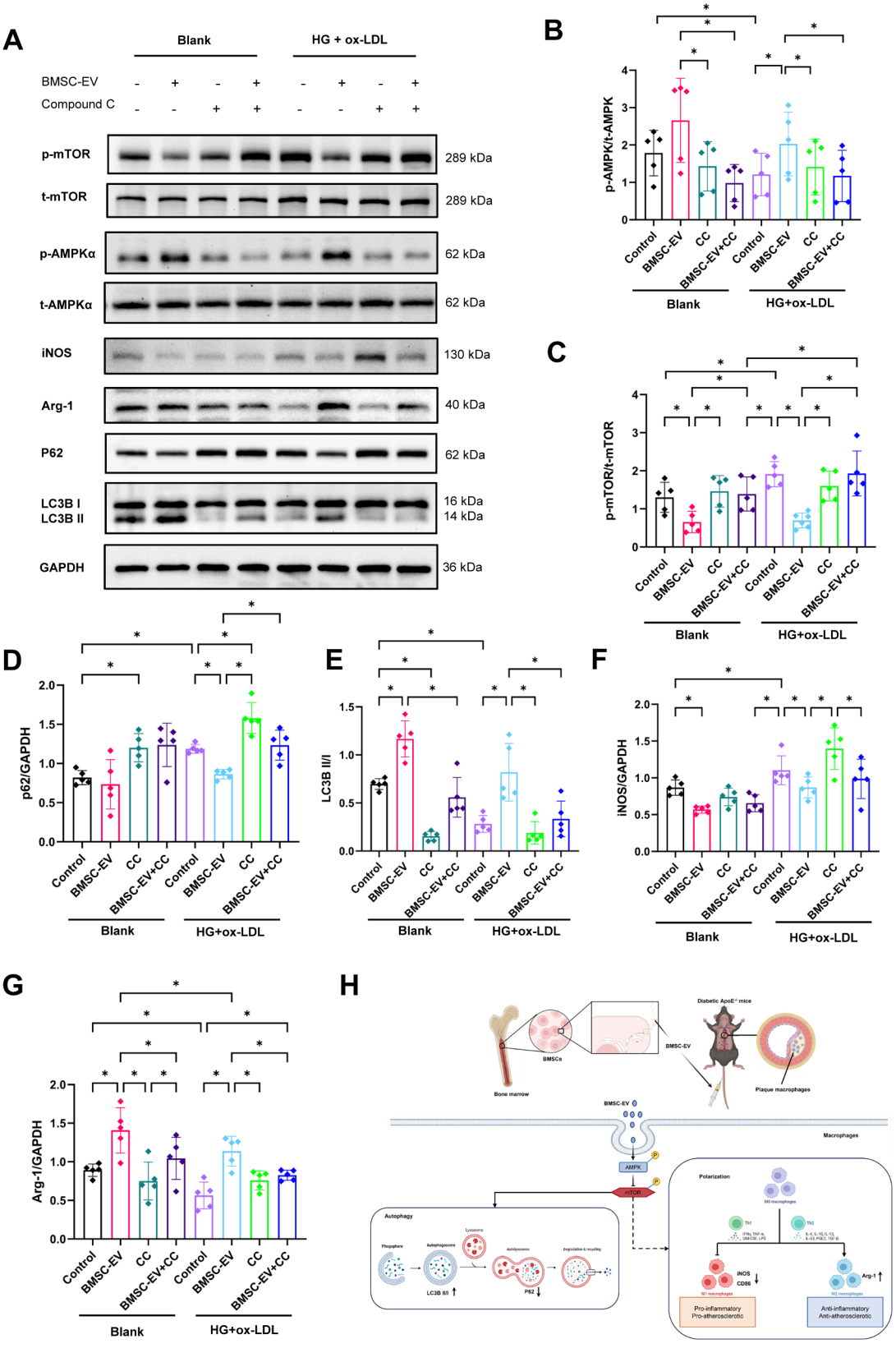

Fig. 7 (See legend on next page.)

(See figure on previous page.)

Fig. 7 BMSC-EV Regulates Macrophage Autophagy and Polarization Phenotype Through the AMPK/mTOR Pathway. **A**–**G** Western blots showing the relative expression and phosphorylation of AMPK/mTOR in RAW264.7 cells induced by HG and ox-LDL, as well as autophagy and polarization marker molecule expression (n = 5). **H** BMSC-EV alleviates diabetes-aggravated atherosclerosis by modulating autophagy-related macrophage polarization via the AMPK/mTOR pathway (Pairwise comparisons between experimental groups were conducted using one-way ANOVA, * $P < 0.05$). Abbreviations: HG, high glucose; ox-LDL, oxidized low-density lipoprotein; BMSC, bone marrow mesenchymal stem cells; BMSC-EV, extracellular vesicles derived from bone marrow mesenchymal stem cells; CC, compound C; p-mTOR, phosphorylated mammalian target of rapamycin; t-mTOR, total mammalian target of rapamycin; p-AMPK α, phosphorylated adenosine monophosphate-activated protein kinase α; t-AMPK, total adenosine monophosphate-activated protein kinase α; iNOS, inducible nitric oxide synthase; Arg-1, Arginase-1; P62, prostacyclin; LC3B, microtubule-associated protein

model group had significant increases in iNOS expression, along with significant reductions in Arg-1 expression (all $P < 0.05$). BMSC-EV treatment reversed iNOS and Arg-1 expression in the model group (both $P < 0.05$) (Fig. 6C).

BMSC-EVs regulate macrophage autophagy and polarization via the AMPK/mTOR Pathway

To understand the mechanism by which BMSC-EVs regulate autophagy and polarization phenotypes RAW264.7 cells, we focused on the AMPK/mTOR pathway, which is known for its role in both autophagy and macrophage polarization. We validated the presence of key molecules in this pathway using western blots. Initially, compared with the untreated group, combination treatment with HG and ox-LDL increased the p-mTOR/t-mTOR ratio, decreased the p-AMPKα/t-AMPKα ratio, elevated iNOS and P62 expression, and reduced Arg-1 and LC3B II/I expression (Blank Control vs. HG+ox-LDL Control, $P < 0.05$). Subsequently, administration of BMSC-EVs in the induction group decreased the p-mTOR/t-mTOR ratio, increased the p-AMPKα/t-AMPKα ratio, reduced iNOS and P62 expression, and increased Arg-1 and LC3B II/I expression compared with the HG + ox-LDL control group (HG + ox-LDL-BMSC-EV group vs. HG + ox-LDL-Control group, $P < 0.05$). Additionally, the AMPK inhibitor Compound C partially blocked BMSC-EV-mediated effects. Specifically, introducing Compound C after BMSC-EV treatment increased the p-mTOR/t-mTOR ratio and decreased the p-AMPKα/t-AMPKα ratio. These changes were also accompanied by increased P62 expression, as well as decreased Arg-1 and LC3B II/I expression (HG + ox-LDL-BMSC-EV group vs. HG + ox-LDL-BMSC-EV + CC group, $P < 0.05$). Unfortunately, no statistically significant changes in iNOS were observed(HG + ox-LDL-BMSC-EV group vs. HG + ox-LDL-BMSC-EV + CC group, $P > 0.05$) (Fig. 7A–G).

Effects of BMSC-EV on liver histopathology

HE staining of mouse livers after 12 weeks of continuous administration showed that, compared with the WT group, the DA group had widely distributed white lipid droplets of varying sizes within hepatocyte cytoplasm. In contrast, BMSC-EV-treated mouse livers showed a reduced number of lipid droplets, and these droplets had a more limited distribution. There were also no apparent structural abnormalities in BMSC-EV group liver tissue (Supplementary Fig. 3).

Discussion

Here, we isolated BMSC-EVs from primary cultured mouse BMSCs. Our primary results demonstrated that BMSC-EVs inhibited macrophage proliferation and migration, reduced foam cell formation in vitro, and attenuated diabetes-exacerbated atherosclerosis in vivo. BMSC-EVs also delayed diabetes-exacerbated atherosclerosis by decreasing macrophage M1 polarization and upregulating autophagy via the AMPK/mTOR pathway (Fig. 7H).

Several mechanisms are involved in the formation of atherosclerosis, including inflammatory pathways, oxidative stress, chronic hyperglycemia and AGEs [18]. Our results also showed that hyperglycemia exacerbated atherosclerosis both in vivo and in vitro. In our in vivo model, ApoE$^{-/-}$ diabetic mice showed more severe atherosclerosis compared to their non-diabetic counterparts. Similarly, in vitro, HG levels increased the percentage of macrophages that formed foam cells in response to ox-LDL.

We isolated nanoscale particles from BMSC supernatant. These particles had characteristics consistent with exosomes in terms of morphology, particle size distribution, and surface molecules. However, due to the limitations of ultracentrifugation, which cannot separate exosomes from other extracellular vesicles, we refer to these elements as EVs (following the recommendations of the International Society for Extracellular Vesicles (ISEV) [19]. Follow-up experimental results showed that BMSC-EV treatment significantly attenuated the degree of atherosclerosis in diabetic ApoE$^{-/-}$ mice, mirroring the effects observed following BMSC treatment. Similar reductions in blood glucose, TC, TG, and LDL levels were observed in mice treated with BMSC-EVs. BMSC-EVs are multifaceted, which can be attributed to the complexity of their molecular contents. Mechanistically, glucose and lipoprotein metabolisms are closely interrelated, and hypoglycemic treatments in diabetic patients can significantly improve their lipoprotein profiles [20]. Notably, BMSC-EV treatment also increased insulin levels in diabetic mice. Previous studies have shown that MSC-EVs promote pancreatic β-cell survival in type 1 diabetes via activation of protective autophagy [14].

Thus, we hypothesize that one of the mechanisms by which BMSC-EVs simultaneously improve serum glucose and lipoprotein levels in diabetic atherosclerotic mice is via enhancement of β-cell survival, which improves glycemic control and subsequently benefits serum lipoprotein profiles.

The potential for BMSC-EVs to exert direct effects on the liver and regulate lipid metabolism also warrants further investigation. Liver histological examination conducted in this study provides preliminary evidence in support of this hypothesis (Supplementary Fig. 3). Interestingly, BMSC-EVs did not induce significant increases in HDL, which may be because distinct metabolic pathways govern HDL and LDL [2].

BMSC-EVs reduce blood glucose and lipid levels, both of which are key factors in atherosclerotic progression. Additionally, in vitro experiments demonstrated that BMSC-EVs can directly inhibit ox-LDL and HG-induced macrophage proliferation, macrophage migration, and foam cell formation. Therefore, BMSC-EV driven attenuation in diabetes-accelerated atherosclerosis may result both from systemic lowering of blood glucose and lipid levels and their ability to regulate the phenotype of macrophages within atherosclerotic plaques.

Macrophages play a crucial role in all stages of atherosclerosis and are considered promising therapeutic targets for ASCVD. Recent studies have highlighted that progression and stability in atherosclerotic plaques are influenced by the number of infiltrating macrophages, their polarization state, and the balance between different macrophage subpopulations [21]. Resting macrophages are termed M0 cells, and classically activated pro-inflammatory M1 cells and alternatively activated anti-inflammatory M2 cells are the two most-studied macrophage polarization phenotypes [22]. Although M1 macrophages exacerbate atherosclerosis, M2 macrophages mitigate it. Previous studies have shown that ox-LDL promotes M1 polarization in atherosclerotic lesions [23]. MSC-EVs may stabilize atherosclerotic plaques by reducing macrophage accumulation and M1 polarization [24], promoting M2 macrophage polarization [25], and inhibiting NLRP3 expression in the arterial wall [26]. Consistent with these findings, we found that BMSC-EV treatment significantly reduced M1 macrophage infiltration in diabetic ApoE$^{-/-}$ mice. In vitro, BMSC-EVs inhibited HG and ox-LDL-mediated macrophage proliferation and migration. BMSC-EVs also downregulated M1 markers, such as iNOS and CD86, while upregulating the M2 marker Arg-1.

This study also attributes the mechanism by which BMSC-EV regulates macrophage polarization to autophagy regulation. In times of metabolic stress, autophagy helps maintain lipid homeostasis and insulin sensitivity, and impaired autophagy has been associated with diabetes [27]. Metabolic abnormalities that impair autophagy promote a pro-inflammatory macrophage phenotype by enhancing M1 macrophage polarization and inhibiting M2 macrophage polarization [28]. Our results are consistent with these previous findings, as we observed diminished autophagy and an increased proportion of M1 macrophages in the HG and ox-LDL environment. Additionally, administration of the autophagy agonist rapamycin significantly reduced M1 macrophage infiltration in diabetic ApoE$^{-/-}$ mice, further supporting the role of autophagy in macrophage polarization. Notably, BMSC-EV treatment upregulated autophagy, inhibiting M1 polarization and promoting M2 polarization. These findings provide valuable insight into the biological mechanisms by which BMSC-EVs mitigate diabetes-exacerbated atherosclerosis.

In the classical autophagy regulation signaling pathway, AMPK phosphorylates and activates ULK1 (UNC-51-like kinase 1), which induces autophagy [29]. The mechanistic target of rapamycin complex 1 (mTORC1), a crucial negative regulator of autophagy, inhibits AMPK function by disrupting the interaction between AMPK and ULK1. Additionally, AMPK alleviates mTORC1-mediated inhibition of autophagy by phosphorylating RAPTOR and the upstream regulator TSC2, which reduces mTORC1 activity [30]. Previous studies have suggested that the mTOR pathway also plays a significant role in regulating macrophage polarization [31]. Thus, mTOR may sit at the intersection of both autophagy and macrophage polarization signaling mechanisms. We used the AMPKα inhibitor compound C to preliminarily verify that BMSC-EVs rely on the AMPK-mTOR pathway to both upregulate macrophage autophagy and induce M2 polarization. These findings further supports the notion that the AMPK/mTOR pathway is a key regulator of macrophage polarization via autophagy, and provides a foundation for investigating the more detailed mechanisms by which BMSC-EVs modulate macrophage phenotypic changes. However, this approach, which is based on literature-driven hypotheses, has certain limitations. For example, the potential involvement of the PI3K/Akt and MAPK/ERK1/2 pathways, which also regulate autophagy, as well as the NF-κB and PPAR-γ pathways, which are closely linked to macrophage polarization, remains unclear. The crosstalk between these pathways and their roles in BMSC-EV-mediated macrophage polarization also warrants further investigation. A more robust strategy would involve using multi-omics approaches to identify candidate proteins and signaling pathways, followed by a detailed exploration of their interactions.

Numerous previous studies have highlighted the significant potential of EVs in disease treatment. EVs serve as natural mediators of intercellular communication and show excellent stability in circulation. Prior work has

also shown that the CD47 marker on exosomes triggers a "don't eat me" signal, protecting them from phagocytosis and limiting their circulatory clearance [32]. EVs, which have membrane structures similar to cellular membranes, can easily cross biological barriers and have inherent targeting properties. For instance, exosomes derived from central nervous system cells can cross the blood–brain barrier and specifically target neurons [33]. In terms of safety, no severe immune responses or toxicity were observed in mice that were repeatedly administered relatively low doses of human cell-derived EVs over an extended period of time [34, 35]. Over 40 clinical trials are currently underway to explore the use of stem cell-derived exosomes for disease treatment [36]. Notably, the FDA recently approved the first MSC-based therapy, Ryoncil (remestemcel-L), for the treatment of steroid-refractory acute graft-versus-host disease, underling the potential of MSC-EV based therapies [37]. However, the inherent complexity of EVs and challenges in scaling up production remain significant barriers to clinical translation, prompting the development of cell vesicle engineering technologies to address these limitations [38].

This study has several limitations. First, EVs transmit signals to target cells through several mechanisms, including receptor-mediated endocytosis and fusion. However, due to limited resources, we were unable to determine the specific mechanisms by which EVs interact with macrophages. Second, atherosclerosis involves multiple cell types from both the circulation and plaque tissues. Further investigation of BMSC-EV effects and mechanisms using different cellular models is needed. Finally, EVs are highly heterogeneous, with differences in size, content, function, and tissue origin. Thus, investigating vesicle-specific content molecules is crucial to fully explore the therapeutic effects of the cellular mechanisms underlying BMSC-EVs.

Conclusions

In conclusion, diabetes inhibits macrophage autophagy and increases M1 macrophage polarization by downregulating AMPK, which aggravates atherosclerosis. BMSC-EVs attenuate diabetes-exacerbated atherosclerosis by inhibiting vascular macrophage proliferation, migration, and foam cell formation. These effects may be mediated via autophagy-associated macrophage polarization, which is regulated by the AMPK/mTOR pathway. BMSC-EVs have strong potential as a therapy for comorbid T2DM and atherosclerosis.

Supplementary Information

The online version contains supplementary material available at https://doi.org/10.1186/s12933-025-02603-0.

Supplementary Material 1

Acknowledgements

This work was supported by The National Natural Science Foundation of China (No. 82100486), the Shandong First Medical University Youth Science Fund Development Program (No.202201-103), the Beijing Hospitals Authority's Ascent Plan (No. DFL20220603) and the High-level public health technical talent construction project of Beijing Municipal Health Commission (Leading Talent-02-01).

Author contributions

X.S. and J.T. conceptualized and designed the study. Research experiments and data analysis were performed by L.L., Z.A., H.Z., and X.W.. The first draft of the manuscript was written by L.L. and Z.A.. All authors read and approved the final manuscript. X.Y., and X.Z. revised the manuscript.

Availability of data and materials

No datasets were generated or analysed during the current study.

Declarations

Competing interest

The authors declare no competing interests.

Author details

[1]Department of Cardiology, Beijing Anzhen Hospital, Capital Medical University, No.2 Anzhen Road, Chaoyang District, 100029 Beijing, China
[2]Department of Cardiology, The Second Affiliated Hospital of Shandong First Medical University, No. 366 Taishan Street, Taishan District, 271000 Tai'an, China

Received: 29 September 2024 / Accepted: 17 January 2025
Published online: 29 January 2025

References

1. Mosenzon O, Alguwaihes A, Leon JLA, Bayram F, Darmon P, Davis TME, Dieuzeide G, Eriksen KT, Hong T, Kaltoft MS, et al. CAPTURE: a multinational, cross-sectional study of cardiovascular disease prevalence in adults with type 2 diabetes across 13 countries. Cardiovasc Diabetol. 2021;20(1):154.
2. Luo Y, Peng D. Residual atherosclerotic cardiovascular disease risk: focus on non-high-density lipoprotein cholesterol. J Cardiovasc Pharmacol Ther. 2023;28:10742484231189596.
3. Zhang Y, Xin W, Hu X, Wang H, Ye X, Xu C, Nan Y, Wu Z, Ju D, Fan J. Inhibition of Hedgehog signaling ameliorates foam cell formation by promoting autophagy in early atherosclerosis. Cell Death Dis. 2023;14(11):740.
4. Shao BZ, Han BZ, Zeng YX, Su DF, Liu C. The roles of macrophage autophagy in atherosclerosis. Acta Pharmacol Sin. 2016;37(2):150–6.
5. Evans TD, Jeong SJ, Zhang X, Sergin I, Razani B. TFEB and trehalose drive the macrophage autophagy-lysosome system to protect against atherosclerosis. Autophagy. 2018;14(4):724–6.
6. Luo Y, Lu S, Gao Y, Yang K, Wu D, Xu X, Sun G, Sun X. Araloside C attenuates atherosclerosis by modulating macrophage polarization via Sirt1-mediated autophagy. Aging (Albany NY). 2020;12(2):1704–24.
7. Xu J, Zhang J, Zhang Z, Gao Z, Qi Y, Qiu W, Pan Z, Guo Q, Li B, Zhao S, et al. Hypoxic glioma-derived exosomes promote M2-like macrophage polarization by enhancing autophagy induction. Cell Death Dis. 2021;12(4):373.
8. Deleyto-Seldas N, Efeyan A. The mTOR-autophagy axis and the control of metabolism. Front Cell Dev Biol. 2021;9: 655731.
9. Xu J, Gao C, He Y, Fang X, Sun D, Peng Z, Xiao H, Sun M, Zhang P, Zhou T, et al. NLRC3 expression in macrophage impairs glycolysis and host immune defense by modulating the NF-κB-NFAT5 complex during septic immunosuppression. Mol Ther. 2023;31(1):154–73.
10. Du Y, Huang F, Guan L, Zeng M. Role of PI3K/Akt/mTOR pathway-mediated macrophage autophagy in affecting the phenotype transformation of lung fibroblasts induced by silica dust exposure. Zhong Nan Da Xue Xue Bao Yi Xue Ban. 2023;48(8):1152–62.

11. Wang X, Wang J, Zhang P, Zhang C, Wang W, Wu M, Xu W, Tao L, Li Z, Zhang Y. Cytotoxicity and autophagy induced by ivermectin via AMPK/mTOR signaling pathway in RAW2647 cells. Molecules. 2023;28(5):2201.
12. Xu X, Gao W, Li L, Hao J, Yang B, Wang T, Li L, Bai X, Li F, Ren H, et al. Annexin A1 protects against cerebral ischemia-reperfusion injury by modulating microglia/macrophage polarization via FPR2/ALX-dependent AMPK-mTOR pathway. J Neuroinflammation. 2021;18(1):119.
13. Kalluri R, LeBleu VS. The biology, function, and biomedical applications of exosomes. Science. 2020;367(6478):eaau6977.
14. Fang J, Chen Z, Lai X, Yin W, Guo Y, Zhang W, Ma J, Li G, Zhang L. Mesenchymal stem cells-derived HIF-1α-overexpressed extracellular vesicles ameliorate hypoxia-induced pancreatic β cell apoptosis and senescence through activating YTHDF1-mediated protective autophagy. Bioorg Chem. 2022;129:106194.
15. Charoenviriyakul C, Takahashi Y, Morishita M, Nishikawa M, Takakura Y. Role of extracellular vesicle surface proteins in the pharmacokinetics of extracellular vesicles. Mol Pharm. 2018;15(3):1073–80.
16. Royo F, Cossío U, Ruiz de Angulo A, Llop J, Falcon-Perez JM. Modification of the glycosylation of extracellular vesicles alters their biodistribution in mice. Nanoscale. 2019;11(4):1531–7.
17. Furman BL. Streptozotocin-induced diabetic models in mice and rats. Curr Protoc. 2021;1(4): e78.
18. Maida CD, Daidone M, Pacinella G, Norrito RL, Pinto A, Tuttolomondo A. Diabetes and ischemic stroke: an old and new relationship an overview of the close interaction between these diseases. Int J Mol Sci. 2022;23(4):2397.
19. Welsh JA, Goberdhan DCI, O'Driscoll L, Buzas EI, Blenkiron C, Bussolati B, Cai H, Di Vizio D, Driedonks TAP, Erdbrügger U, et al. Minimal information for studies of extracellular vesicles (MISEV2023): from basic to advanced approaches. J Extracell Vesicles. 2024;13(2):e12404.
20. Edwards IJ, Terry JG, Bell-Farrow AD, Cefalu WT. Improved glucose control decreases the interaction of plasma low-density lipoproteins with arterial proteoglycans. Metabolism. 2002;51(10):1223–9.
21. Eshghjoo S, Kim DM, Jayaraman A, Sun Y, Alaniz RC. Macrophage polarization in atherosclerosis. Genes (Basel). 2022;13(5):756.
22. Mouton AJ, Li X, Hall ME, Hall JE. Obesity, hypertension, and cardiac dysfunction: novel roles of immunometabolism in macrophage activation and inflammation. Circ Res. 2020;126(6):789–806.
23. Tabas I, Bornfeldt KE. Intracellular and intercellular aspects of macrophage immunometabolism in atherosclerosis. Circ Res. 2020;126(9):1209–27.
24. Takafuji Y, Hori M, Mizuno T, Harada-Shiba M. Humoral factors secreted from adipose tissue-derived mesenchymal stem cells ameliorate atherosclerosis in Ldlr-/- mice. Cardiovasc Res. 2019;115(6):1041–51.
25. Li J, Xue H, Li T, Chu X, Xin D, Xiong Y, Qiu W, Gao X, Qian M, Xu J, et al. Exosomes derived from mesenchymal stem cells attenuate the progression of atherosclerosis in ApoE(-/-) mice via miR-let7 mediated infiltration and polarization of M2 macrophage. Biochem Biophys Res Commun. 2019;510(4):565–72.
26. Lin Y, Liu M, Chen E, Jiang W, Shi W, Wang Z. Bone marrow-derived mesenchymal stem cells microvesicles stabilize atherosclerotic plaques by inhibiting NLRP3-mediated macrophage pyroptosis. Cell Biol Int. 2021;45(4):820–30.
27. Gonzalez CD, Lee MS, Marchetti P, Pietropaolo M, Towns R, Vaccaro MI, Watada H, Wiley JW. The emerging role of autophagy in the pathophysiology of diabetes mellitus. Autophagy. 2011;7(1):2–11.
28. Liu K, Zhao E, Ilyas G, Lalazar G, Lin Y, Haseeb M, Tanaka KE, Czaja MJ. Impaired macrophage autophagy increases the immune response in obese mice by promoting proinflammatory macrophage polarization. Autophagy. 2015;11(2):271–84.
29. Kim J, Kundu M, Viollet B, Guan KL. AMPK and mTOR regulate autophagy through direct phosphorylation of Ulk1. Nat Cell Biol. 2011;13(2):132–41.
30. Herzig S, Shaw RJ. AMPK: guardian of metabolism and mitochondrial homeostasis. Nat Rev Mol Cell Biol. 2018;19(2):121–35.
31. Byles V, Covarrubias AJ, Ben-Sahra I, Lamming DW, Sabatini DM, Manning BD, Horng T. The TSC-mTOR pathway regulates macrophage polarization. Nat Commun. 2013;4:2834.
32. Kamerkar S, LeBleu VS, Sugimoto H, Yang S, Ruivo CF, Melo SA, Lee JJ, Kalluri R. Exosomes facilitate therapeutic targeting of oncogenic KRAS in pancreatic cancer. Nature. 2017;546(7659):498–503.
33. Vader P, Mol EA, Pasterkamp G, Schiffelers RM. Extracellular vesicles for drug delivery. Adv Drug Deliv Rev. 2016;106(Pt A):148–56.
34. Mendt M, Kamerkar S, Sugimoto H, McAndrews KM, Wu CC, Gagea M, Yang S, Blanko EVR, Peng Q, Ma X, et al. Generation and testing of clinical-grade exosomes for pancreatic cancer. JCI Insight. 2018;3(8):e99263.
35. Zomer A, Maynard C, Verweij FJ, Kamermans A, Schäfer R, Beerling E, Schiffelers RM, de Wit E, Berenguer J, Ellenbroek SIJ, et al. In Vivo imaging reveals extracellular vesicle-mediated phenocopying of metastatic behavior. Cell. 2015;161(5):1046–57.
36. Tan F, Li X, Wang Z, Li J, Shahzad K, Zheng J. Clinical applications of stem cell-derived exosomes. Signal Transduct Target Ther. 2024;9(1):17.
37. Murata M, Teshima T. Treatment of steroid-refractory acute graft-versus-host disease using commercial mesenchymal stem cell products. Front Immunol. 2021;12: 724380.
38. de Abreu RC, Fernandes H, da Costa Martins PA, Sahoo S, Emanueli C, Ferreira L. Native and bioengineered extracellular vesicles for cardiovascular therapeutics. Nat Rev Cardiol. 2020;17(11):685–97.

Publisher's Note